Anthropocene Coasts

RESEARCH ARTICLE

Open Access

Hydrodynamics and sediment transport patterns on intertidal flats along middle Jiangsu coast

Fei Xing[1], Ya Ping Wang[1,2*] and Jianjun Jia[1]

Abstract

Two field campaigns in Dafeng and Jianggang were organized to compare spatial variations of hydrodynamic characteristics and sediment transport patterns on intertidal flats of different types with distinct human interferences along middle Jiangsu coast, China. The major contributors to the different patterns of sediment dynamics between the two tidal flats were offshore tidal current field and human interference. Offshore tidal force provide the basic setup of tidal current patterns on tidal flats, which is then modified by local morphology. Seawalls parallel to coast reduce tidal flat width, forcing tidal energy to dissipate within a shorter distance and thus influencing tidal flat morphology. Seawalls vertical to coast and major tidal current significantly reduce tidal current speed, which favors sediment deposition on tidal flats. Two seawalls built on both sides of the observational tidal flat profile caused much reduced current speed at Dafeng tidal flat, comparing to the offshore station. Being exposed to offshore radial tidal currents, hydrodynamics at Jianggang was much stronger than that at Dafeng. Residual currents at both areas showed net landward transport at the lower flat and net seaward transport at the upper flat, in favor to sediment accumulation at the middle flat. Sediment flux over tidal cycles showed net landward sediment transport at Dafeng, and net seaward transport at Jianggang, consistent with the convex-up accretion-dominated profile observed at Dafenge, and concave-up erosion-dominated profile observed at Jianggang. The instantaneons sediment flux changed significantly due to variations in velocity and sediment concentrations, but these terms counteracted with each other within tidal cycles, leading to the dominant role of Eulerian flux in determining net sediment flux over tidal cycles.

Keywords: Hydrodynamics, Sediment flux, Land reclamation, Tidal flat, Jiangsu coastal ocean

1 Introduction

Tidal flat is a morphological unit commonly found along coasts where tides are the dominant force with abundant fine sediment supply. With tens of kilometers in width and gentle slope, tidal flats serve as a great buffer against coastal hazards (coastal storms, high wave events, and flooding) (Wang and Ke 1997; Murray et al. 2012; Jin et al. 2017; Zhang et al. 2021), which also provide home for massive wetland species (Barbier et al. 2008; Koch et al. 2009; Ghosh et al. 2016). When there are plenty of sediment supply, tidal flats prograde fast into the ocean, forming massive valuable land resource (Wang et al. 2020). On the other hand, with reduced sediment supply, global sea level rise and human reclamation projects, some tidal flats and associated wetlands are facing severe erosion, putting human behind them under high risk (Zhao et al. 2022). Morphodynamics of tidal flat systems have been widely studied around the world, providing us a comparatively complete figure on mechanisms controlling hydrodynamics, sediment transport patterns, and correlated morphological changes on tidal flats (Friedrichs and Aubrey 1996; Eisma 1997; Le Hir et al. 2000;

*Correspondence: ypwang@nju.edu.cn

[2] Ministry of Education Key Laboratory for Coast and Island Development, School of Geographic and Oceanographic Sciences, Nanjing University, Nanjing 210093, China
Full list of author information is available at the end of the article

Friedrichs 2011; Zhou et al. 2022). Tidal flats vary significantly in properties, but they share some common characteristics. For instance, tidal flats are usually classified into supratidal, intertidal and subtidal zones based on tidal levels, and the major hydrodynamic factors influencing tidal flats are tides, winds, waves, density-driven circulation and drainage processes (Le Hir et al. 2000). These forces have distinct influences on tidal flat morphology, moving fine sediment to the supratidal flat and coarse sediment to subtidal flat, forming spatial variations of sediment grain size from upper to lower tidal flats (Wei et al. 2020). Accretion-dominated tidal flats tend to be high and convex-up while erosion-dominated tidal flats are low and concave-up, and the shapes of tidal flat profile adjust to variations of different drivers (Kirby 2000; Friedrichs 2011). Sediment supply and composition, tidal range, bed slope, human projects, and vegetation are the major contributors to tidal flat morphology (Gao 2009).

Tidal flats along Jiangsu coastal ocean in China are unique, as their large scales (with a mean width of about 8 km), plenty fine-grained sediment supply from Changjiang and Yellow river, and the geomorphologic assemblage of coastal tidal flats and an offshore radiant sand ridge field. The special hydrodynamics and morphology are attractive to a lot of researchers. Been first studied in detail since the 1980s (Wang 1983; Ren 1986; Zhang 1986), there had been a lot of field investigations and research on tidal current patterns, sediment transport and evolution processes in this area (Ke and Yu 1990; Wang and Zhu 1990; Wang et al. 2012; Zhou et al. 2022). In addition, tidal flats have provided massive land resource in China, which prograde probably 50-100 m/year in the north part of the Jiangsu coast (Ren 1984). High tidal flats (150 cm above mean sea level) along Jiangsu coast have accumulated and been reclaimed at an average rate of 115.9 m/yr between 1976 to 2016 (Wang et al. 2020). The reclamation of tidal flats reduces width of flats, and destroys the former tidal flat profile equilibrium. 16.61×10^4 hm^2 of tidal flats have been reclaimed since 1984 in Jiangsu province (Xu et al. 2022), which became the predominant factor controlling the morphological evolution of tidal flats in this area. As a result, massive tidal flats are experiencing profile adaption. Land reclamation activities have stopped since 2020, but these tidal flat systems are still undergoing massive morphological changes to achieve their equilibrium. Massive studies are focused on the morphodynamics of tidal flat systems along Jiangsu coast (Wang and Ke 1997; Wang et al. 1999, 2006a, b; Gao 2009), but there are still far from enough to understand the mechanisms how morphology responds to varied hydrodynamics and human activities. Along China coast, tidal flats have experienced significant morphological changes over the recent decades due to land reclamation. The undergoing tidal flat morphological evolution along Jiangsu coast provides us a great opportunity to learn the interactions of hydrodynamics and morphodynamics on tidal flats under the influences of both natural and anthropogenic factors, which will deepen our insights on predicting morphological evolution of tidal flat systems and provide us meaningful suggestions on making sustainable coastal management plans.

The purpose of this study is to analyze hydrodynamics and corresponding sediment transport patterns along two tidal flats located in different areas along a deep channel (Xiyang) which have similar sediment sources, but encounter different offshore hydrodynamic setup and human interferences. The distinctive characteristics of tidal flats in these two areas provide us more clues on understanding the mechanisms of sediment dynamics on tidal flats.

2 Regional setting

Two tidal flats, located in Dafeng, and Jianggang, on the land side of Xiyang deep channel were chosen as our study areas to compare the differences in tidal flat morphodynamics (Fig. 1). Xiyang deep channel is one of the largest tidal channels in the radical sand ridge system offshore of Jiangsu coast. The sand ridge system is composed of more than 70 sand ridges and tidal channels, formed by the progressive tidal wave system propagating from the East China Sea interacting with a rotational tidal wave system approaching from the southern Yellow Sea along Jiangsu coast. The two tidal wave systems form a rotational tidal current field, with its center located at Jianggang (Li et al. 1979; Li and Zhao 1995). Semi-diurnal tidal flow is dominant in this area, and tidal currents have significant spatial variations. Bi-directional current with low ellipticity is dominant in the north of Jianggang, from where tidal current gradually changes into a rotatory pattern with increasing ellipticity toward the south (Xing et al. 2012). According to average tidal range, tidal flats along Jiangsu coast are classified into two types: strong tidal coast, which extends from Jianggang to Beikan with the average tidal range of larger than 4 m; and middle tidal coast, extends southwards from Beikan and northwards of Jianggang with the average tidal range of 2 - 4 m (Zhang 1986; Dionne 1988). Dafeng is located in the middle tidal zone, facing Xiyang deep channel, where the deepest point is more than 20 m (Zhang 1986). Tidal creeks are relatively sparse and mostly extend vertically to shoal line (Fig. 1b). On the other hand, Jianggang is located on the south end of the Xiyang channel, at the converging point where several large channels distributed radically with strong hydrodynamics and rapid

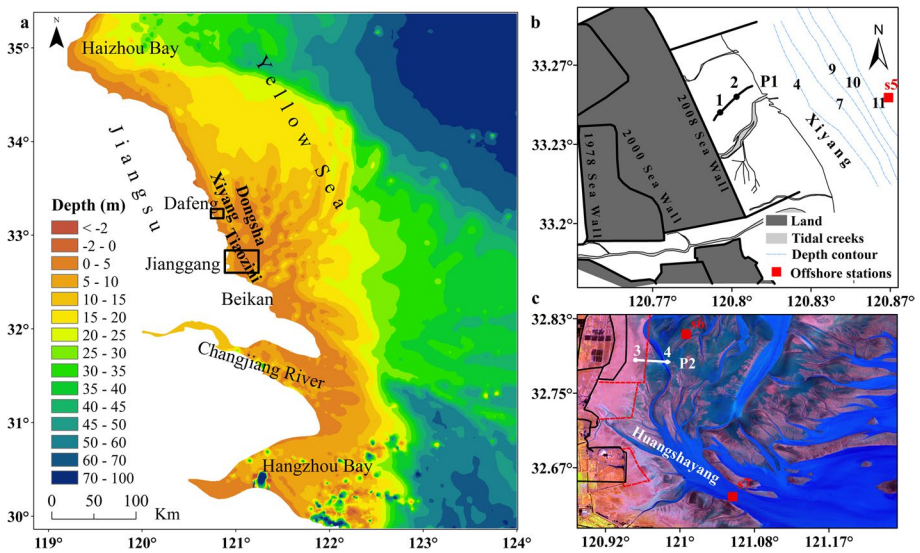

Fig. 1 **a** Locations of study areas showing two tidal flats and the radical sand ridge systems; **b** topology, sampling stations and profile along Dafeng tidal flat; and **c** topology, sampling stations and profile along Jianggang tidal flat. In **b**, black lines along coast represent seawalls that have been built since 1978; black points display the location of observational stations (1 and 2) and black line along the tidal flat (P1) shows the profile along which elevation and bed surface sample data were collected. Red square (s5) is the offshore station from which offshore hydrodynamic parameters (water depth and velocities) were derived from a validated Delft3D model (Ni 2014). In **c**, black lines along coast represent seawall built before 2009 and red lines show seawall built in 2012 and 2013 after our field trip; white points along the white line demonstrate the location of observational stations along the tidal flat profile, where elevation and bed surface sample data were collected, respectively. Red squares (s6 and s7) show the location where offshore hydrodynamic parameters (water depth and velocities) were derived from a validated Delft3D model (Ni 2014)

morphological changes. Jianggang tidal flat is characterized with complicated topography and multiple tidal creeks, which extend mostly parallel to the shoal (Fig. 1c). Seawalls are widely distributed on the land side of tidal flats along Jiangsu coast. Several seawalls have been constructed along Dafeng tidal flat, in 1978, 2000, and 2008, largely shortened the width of tidal flat from larger than 10 km in 1978 to 2.9 km at 2008 (Wang et al. 2012). Besides, two seawalls have been built perpendicular to shoreline on both side of our observation profile in the Dafeng tidal flat. Sediment properties are similar in these two areas as they have similar sediment sources from abandoned Yellow River and Changjing River deposits (Ren 1986; Zhang 1992). Silt and sandy silt are the main components of surface sediment on these tidal flats (Wang and Ke 1997).

Jiangsu coastal area is controlled by subtropical monsoon climate with annual mean temperature of 14 ~ 20 degree and mean annual precipitation of 1000 ~ 1200 mm (Ren et al. 1985; Ke et al. 1990). Southwest winds dominate in summer and northeast winds dominate in winter. Winter storms happen frequently in winter and spring from October to May, which is the windiest time of a year. Significant wave height is generally smaller than 1.0 m in winter and less than 0.5 m in other seasons (Xing et al. 2012). Although winds and related high waves can significantly influence tidal flat morphology within a short time period (Bartholdy and Aagaard 2001; Xie et al. 2017), tides are still the most dominant force controlling tidal flat evolution.

3 Methods

3.1 Field trip and laboratory analysis

We organized two field trips on tidal flats along the middle Jiangsu coast, one in Dafang from Apr. 20th to Apr. 23nd, 2009, and the other in Jianggang from Oct. 5th to Oct. 10th, 2009 (Fig. 1), during spring and autumn, when these tidal flats are under typical hydrodynamic conditions with minor impact from extreme events, such as storms. Two stations were designed along each of the tidal flat profile, with an Acoustic Doppler Velocimeter (ADV-OCEAN) and an optical backscatter sensors of OBS (D&A Instrument Company, USA) placed at the upper flat of the intertidal zone (station 1 in Fig. 1b and station 3 in Fig. 1c, at station 1 no OBS was deployed). An Acoustic Doppler Current Profiler (ADCP) was deployed on the lower flat close to the mean low water level line (station 2 in Fig. 1b and station 4 in Fig .1c) to obtain current velocity of each water layer with vertical resolution of 0.05 m. At station 1, the ADV measured current velocity at 0.18 m above the bottom with a burst interval of 2 min in autonomous

deployment mode for 64 s at a frequency of 4 Hz. At station 3, the ADV measured velocity at 0.23 m above bed with the same settings as that in Dafeng. The OBS was set up at 0.12 m above bed with working frequency of 1 Hz and 20 samples per burst with interval of 5 min. During both field trips, ADCPs were set to measure vertical velocity profiles with sampling frequency of 1 Hz and burst interval of every 1 min. At the meantime, water samples were collected using a tube sampler lay vertically to the sea floor with sampling interval of 1 h at both station 2 and 4 for further analysis in the laboratory. ADCPs started to record valid data when water depth was larger than about 0.7 m, on the other hand, ADVs and OBS started working when they were submerged. In addition, bed elevation data and surface sediment samples were acquired along profile P1 (Fig. 1b) and P2 (Fig. 1c) with a Global Position-finding system Real Time Kinematic (GPS-RTK) when water level was close to the low water line. The position of all stations and sampling points were determined with the GPS-RTK.

The collected water samples were analyzed in the laboratory to get suspended sediment concentrations (SSCs, mg/L) at station 2, 3 and 4 through a process involving filtering with pre-weighted paper filters and oven-drying at a temperature between 40 and 50 °C. Using the field collected water and suspended sediment, solution with different SSCs were prepared. OBS and ADCPs were set to record data for different SSCs. Meanwhile, water samples were collected, filtered, and dried to get realistic SSCs. Linear regression relationships were then found between OBS turbidity, ADCP backscatter strength and realistic SSCs (Fig. 2). Applying the linear regression coefficients, field collected turbidity data recorded by OBS at station 3, vertical profiles of backscatter strength recorded by ADCP at station 2 and 4 were converted to SSCs. Meanwhile, particle size measurements were carried out for water samples with a Mastersizer 2000 laser granulometer (Malvern Instrument Ltd.; measuring range of 0.02 ~ 2000 um; particle size resolution of 0.01 ϕ, reproducibility error of < 3%). SSCs and velocities were used to calculate vertical mean velocities (station 1 and 3) and SSCs (station 3) by means of the modified Hardisty equation from Wang and Gao (2001) to calculate residual current and residual sediment flux. The area within blanking distance of ADCP was made up with Logarithm profile equation.

3.2 Residual current and residual sediment flux calculation

Residual current and sediment flux are calculated with Dyer's theory (Dyer 1997). Tidal current velocity (u) are decomposed into three terms: tidal mean velocity (U), tidal variation deviation (u_t) and vertical variation deviation (u_v), shown as:

$$u = U + u_t + u_v \tag{1}$$

Similarly, SSCs (c) can be decomposed into three terms:

$$c = C + c_t + c_v \tag{2}$$

Residual current caused mean water flux over the tidal cycle is shown as:

$$Q = \frac{1}{T}\int_0^t \int_0^1 u \cdot h dz dt = U \cdot H + < \mathrm{u_t} \cdot \mathrm{h_t} >= h \cdot \left(\mathrm{u_E} + \mathrm{u_S}\right) = h \cdot \mathrm{u_L} \tag{3}$$

where u_E, u_L, and u_S indicates mean Eulerian velocity, mean Lagrangian velocity and Stocks drift, respectively. Lagrangian velocity can be described as the sum of Eulerian velocity and Stocks drift. Water depth (h) is decomposed into mean water depth over the tidal cycle (H) and its tidal variations (h_t).

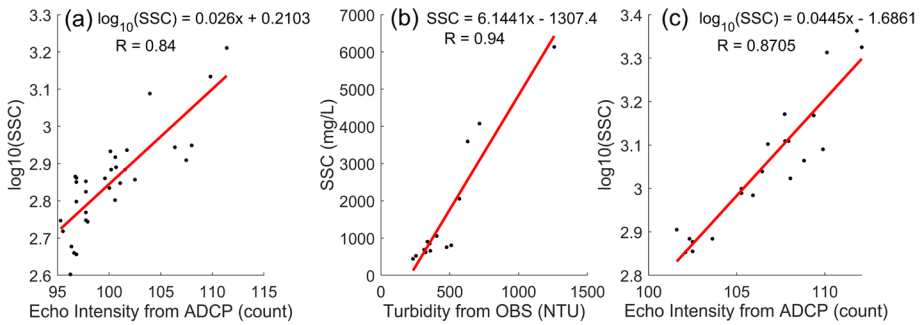

Fig. 2 Calibration curves to convert **a** ADCP echo intensity to SSC (mg/l) at station 2; **b** OBS turbidity (NTU) to SSC (mg/l) at station 3; **c** ADCP echo intensity to SSC (mg/l) at station 4

Applying the same method, the averaged sediment flux (F) over one tidal cycle is expressed with mean, tidal and deviation components:

$$< F >= H \cdot U \cdot C + C \cdot < h_t \cdot \bar{u}_t > + U \cdot < h_t \cdot \bar{c}_t > + H \cdot < \bar{c}_t \cdot \bar{u}_t > + < h_t \cdot \bar{c}_t \cdot \bar{u}_t > + H \cdot < \overline{c_v \cdot u_v} > + < \overline{h_t \cdot c_v \cdot u_v} > = T1 + T2 + T3 + T4 + T5 + T6 + T7 \quad (4)$$

where angled brackets (< >) indicate the mean value over water depth. In Eq. 4, *T1* represents sediment flux due to non-tidal drift deriving from Eulerian velocity; *T2* shows sediment flux produced by Stokes drift; the sum of the first two terms is advective sediment flux. *T3*, *T4*, *T5* are caused by phrase differences and lags between sediment concentrations and velocities; *T6* is related to vertical gravitational circulation, due to the interactions of velocity direction and varying vertical sediment concentrations (important in estuaries, but vary small on intertidal flats); term 7 (*T7*) demonstrates sediment flux from the changing forms of vertical profiles of velocity and concentration, attribute to sour and settling lags.

Suspended sediment instantaneous flux can be decomposed into 5 terms:

$$E = \int_0^1 h \cdot u \cdot c \cdot dz = h \cdot u \cdot c + h \cdot u \cdot c_t + h \cdot u_t \cdot c + h \cdot u_t \cdot c_t + h \cdot u_v \cdot c_v = E1 + E2 + E3 + E4 + E5 \quad (5)$$

where *E1* shows sediment flux caused by mean current; *E2, E3* are caused by tidal variations and correlation of velocity and suspended sediment distributions; *E4* demonstrates sediment transport from tidal pulsation; and *E5* is related to vertical shear stress and diffusion (Dyer 1997).

4 Results

4.1 Hydrodynamics

4.1.1 Dafeng hydrodynamics

Our field observation at Dafeng tidal flat recorded hydrodynamic and sediment transport related parameters for 3-5 successive tidal cycles between the period from neap to spring tide (3 tidal cycles at station 2 and 5 tidal cycles at station 1, station 1 was only submerged for 3 big tidal cycles, Fig. 3). The main character was shown as a small tide following a large tide, caused by tidal deformation in shallow water. At the lower tidal flat (station 2), the observed small tide had the maximum water depth of 0.79 m and highest velocity of 0.22 m/s, comparing to 1.54 m and 0.52 m/s for the neighboring large tide. Located 969 m landward of station 2, the elevation of station 1 was 0.95 m higher than that of station 2. As a result, the upper flat station 1 was submerged only during large tides. Station 2 at the lower flat was dominated by reciprocating flow, which flowed southward during flood tides and northward during ebb tides, with a small western component all over tidal cycles. On the other hand, station 1 was dominated by rotatory currents which mostly flowed northward over all tidal cycles with western landward component during flood tides, and eastern seaward component during ebb tides, which may be influenced by shallow water effect, local topography and existence of seawalls. The maximum tidal current during large tides decreased from 0.52 m/s to 0.24 m/s from station 2 to station 1, due to tidal energy dissipation and the increasing bed shear stress landwards with decreasing water depth (Zhang 1986). In order to show more details of the depth averaged flow features, hydrodynamics over one big tidal cycle was analyzed for the two stations (Fig. 3 red dash rectangles). The major flow axis at station 2 was 13–193°. The average current speed during flood tide was 0.12 m/s, which increased to 0.30 m/s at ebb tide, probably because of the current conflux at ebb. The maximal flood current of approximate 0.31 m/s appeared when water level was about 1.1 m, on the other hand, the maximal ebb current of 0.52 m/s occurred when water level was about 0.89 m. The current speed reduced to zero (about 0.03 m/s) and the current direction began to change from south to north approximately half an hour before the flood slack, demonstrating that the tide wave system was the mixed wave of standing oscillations and progressive wave (Wang et al. 2006b). Current directions deviated to west almost all over the tidal cycle, favors to landward sediment transport. SSCs ranged from 0.43 to 1.33 kg/m^3 during the tidal cycle. Although SSCs have very small temporal variations, the maximum SSC occurred simultaneously with the maximum ebb current, while the extreme high values of SSC at the beginning and ending points of the tidal cycle were the result of tidal intrusion front, related to the high changing rate of water level, showing as the high slope presenting in Fig. 3a (Wang et al. 1999, 2006b). At station 1, the duration of flood and ebb tides were similar, for around 1.5 h. The ebb tide had slightly larger velocities than the flood tide, with the average value of 0.05 m/s at ebb compared to 0.03 m/s at flood. Comparing to station 2, tidal current at station 1 was smaller and unsteady, attributes to small water depth.

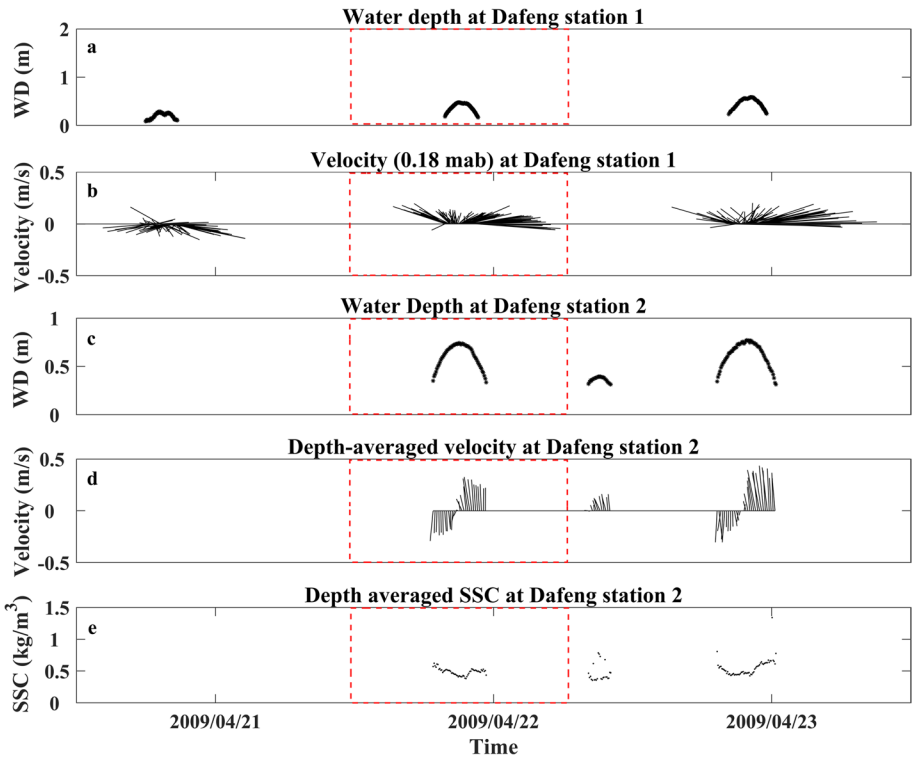

Fig. 3 Time series of water depth, velocities and SSCs at two stations along Dafeng intertidal flat from Apr. 21st to Apr. 23rd, 2009. **a** water depth (m) at station 1; **b** current velocity (m/s) at 0.18 m above sea bed (mab) at station 1; **c** water depth (m) at station 2; **d** vertical averaged current velocity (m/s) at station 2; **e** vertical averaged SSCs (kg/m^3) at station 2. Red dash rectangles show the tidal cycle for which parameters are analyzed in details

The vertical and temporal variations of tidal currents and SSCs at station 2 for the tidal cycle on April. 22, 2009 were derived from ADCP (Fig. 4). Tidal current was decomposed into 193° as the major current axis and 283° as the minor current axis, showing a reciprocating flow pattern. Comparing to the flood tide, the ebb current was stronger and current speed was higher than 0.4 m/s when water depth exceeded 0.5 m. The maximum velocity at ebb was larger than 0.6 m/s close to water surface. On the other hand, flood current was smaller with peak values (larger than 0.3 m/s) occurring occasionally close to water surface, and the maximum velocity was less than 0.4 m/s. Besides, velocity close to sea floor was also larger during ebb tides, consistent with the larger SSCs near seabed during the ebb tide comparing to that during the flood tide. Velocity in the minor direction was limited to 0.15 m/s in magnitude. Tidal current was deviated to west at the first 3.7 h (70% of time of the tidal cycle), which changed to eastward in the last 1.5 h.

SSCs at station 2 were larger at bottom than at surface and the maximum SSCs occurred concurrently with high current speed, showing seabed was the major sediment source (Fig. 4c). The average and maximal values of SSC were higher during the ebb tide, favors to more sediment transport during ebb than flood. The 0.6 kg/m^3 contour line covered the entire tidal cycle with a U shape, showing large SSCs at the beginning and ending of the tidal cycle over the whole water column, which decreased significantly to water surface close to flood slack. This may be correlated to the high current speeds combined with small water depth, favors to sediment mixing.

4.1.2 Jianggang hydrodynamics

The observation at Jianggang tidal flat was conducted at the two stations from spring to neap tidal cycle for 7 tides (Fig. 5). Comparing to Dafeng, water depth and velocities at the two stations were all larger at Jianggang tidal flat., Velocity changed landward from reciprocating flow (Fig. 5e, station 4) to rotatory flow (Fig. 5b, station 3), similar to Dafeng tidal flat. Similar magnitude of tidal range between neighboring tidal cycles shows smaller intertidal asymmetry than Dafeng tidal flat (Fig. 3). SSCs were much higher at Jianggang tidal flat, to be as high as 5 kg/m^3 at station 3 (0.23 mab, Fig. 5c) and around 7 kg/

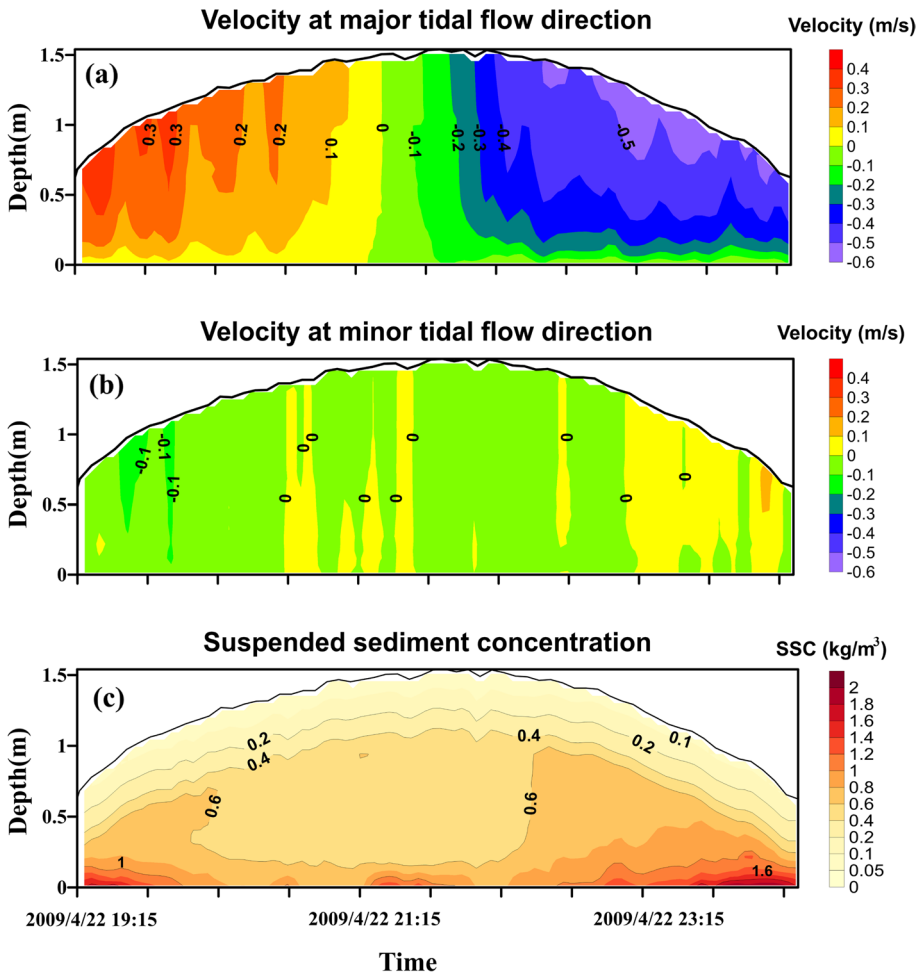

Fig. 4 Time series of velocity and SSC vertical profiles at station 2. **a** tidal current velocity (m/s) at major flow direction (193° from north), **b** tidal current velocity (m/s) at minor flow direction (283° from north); **c** SSCs in kg/m^3

m^3 close to seabed at station 4 (Fig. 6c, comparing to less than 1 kg/m^3 at station 2), indicating sediment dynamics was more active at Jianggang stations.

To check the detailed hydrodynamics over one tidal cycle, data from 23:26 Oct. 7th to 5:40, Oct. 8th, 2009 were analyzed (Fig. 5 red dash rectangle). Station 4 located on the lower flat was characterized with reciprocating current, with the major current axis southward during flood and northward during ebb (351–171°). The ebb tide lasted 1.6 h longer than the flood tide. Correspondingly, the magnitude of current speed during the flood tide was much larger than that during the ebb tide, and the maximum velocity was 1.38 m/s during the flood tide and 0.92 m/s during the ebb tide. The changing rate of tidal current was faster during the flood tide which kept steady during the ebb tide, leading to a slightly larger mean ebb current of 0.70 m/s, than the mean flood current of 0.67 m/s. Current speed reached its minimum of 0.09 m/s about 0.45 h before flood stack, indicating that tidal current was also the mixed wave of progressive wave and standing oscillations. Similar as Dafeng tidal flat, both tidal current and SSCs presented large values at the beginning and ending of the tidal cycle, showing the significant influence from tidal intrusion on both tidal flat systems. Following the variations of velocity, SSCs also showed high values with fast changes during the flood tide, indicating tidal current controlled sediment initiation and movement and that seabed sediment resuspension was the major source for suspended sediment. Comparing to the lower tidal flat, station 3 presented a similar tendency in temporal variations of water depth and current velocities but showing a more obvious rotatory wave pattern. The asymmetry between flood and ebb tides was large, illustrating as the larger time difference between the ebb and the flood tides (2.50 h at station 3 vs. 1.6 h at station 4). At the meantime, current speed during

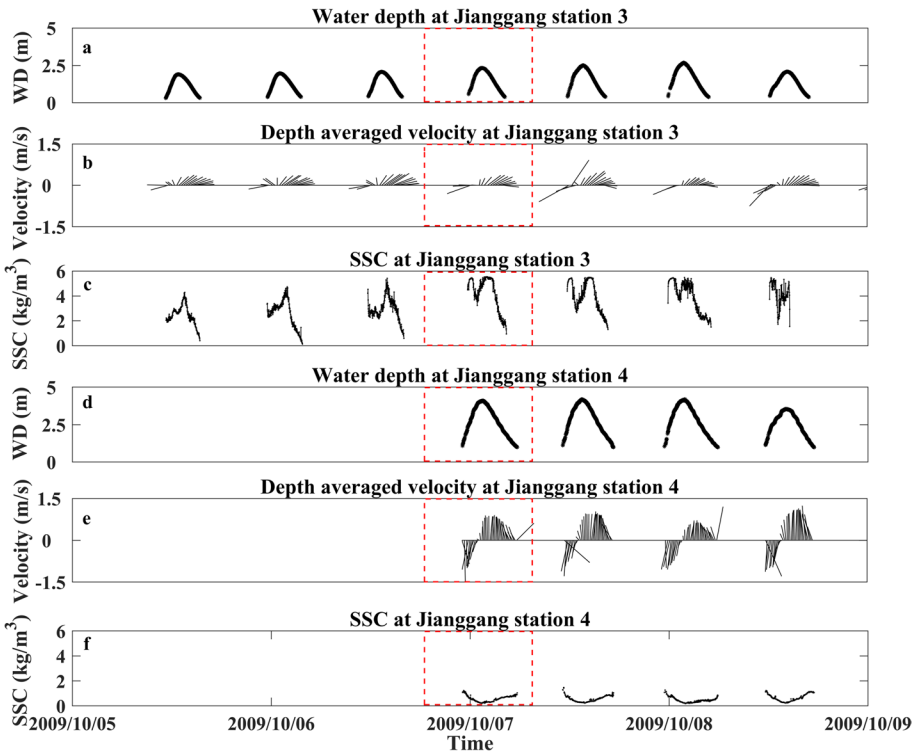

Fig. 5 Time series of depth, velocity and SSCs at two stations on Jianggang tidal flat. **a** water depth at station 3; **b** velocity at 0.23 m above seabed (mab) at station 3; **c** SSCs at 0.12 mab at station 3; **d** water depth at station 4; **e** depth averaged velocity at station 4; **f** depth averaged SSCs at station 4. Red dash rectangles show the tidal cycle that has been analyzed in detail

the flood tide was much smaller than that during the ebb tide, with the maximum of 0.85 m/s and 0.96 m/s, respectively. Velocities switched from westward during the flood tide to eastward during the ebb tide, with the major west-east direction. Peak SSCs occurred shortly after current changed its direction during ebb tides, inconsistent with station 4 where peak SSCs close to bottom occurred during the flood tide (Figs. 5e and 6c).

The ADCP recorded vertical variations of tidal currents and corresponding SSCs over one tidal cycle at station 4 (Fig. 6) showed a comparatively different picture as station 2 (Fig. 4). Tidal current were decomposed into major and minor directions, and the major axis was 351° from north. The flood tide was characterized with larger velocity (maximum velocity of 1.85 m/s) which lasted shorter time, comparing to the ebb tide (maximum velocity of 1.43 m/s). Flood velocities that were larger than 1 m/s lasted for more than 1 h at about 0.6 mab in the flood phase, which were between 0.6 ~ 0.8 m/s at the corresponding layer during the ebb tide. Velocities in the minor axis were kept lower than 0.1 m/s over the tidal cycle except at the beginning and ending period when the instrument was initially submerged. Flood slack when velocity was close to 0 m/s lasted less than half an hour, much shorter than that at Dafeng stations (Fig. 4a).The vertical variations of SSCs at station 4 was alike to that at station 2, in terms of the much higher values close to bottom than that at surface, but SSCs at Jianggang station decreased fast from seabed to water surface, which might be related to the fast changes in vertical velocity profile. SSCs larger than 0.6 kg/m^3 was close to water surface in the flood phase, but was limited to bottom in the ebb phase, consistent with higher velocities during the flood tide. The very high SSCs were limited to water bottom where major velocity was smaller than 0.4 m/s, may be related to vertical stratification. SSCs were as high as 6 kg/m^3 at water bottom, but changed to be smaller than 1 kg/m^3 above 0.5 mab, which decreased to less than 0.2 kg/m^3 at water surface.

4.2 Residual current

Using Dyer's equation, residual currents were calculated for the four stations (Table 1). Eulerian residual currents were the predominant component of Lagrangian residual currents, and Stocks drifts were one magnitude smaller than Euler residual currents (except at station 3). Stocks drift had the same directions as Eulerian residual current (except station 4) at Dafeng and Jianggang tidal flats,

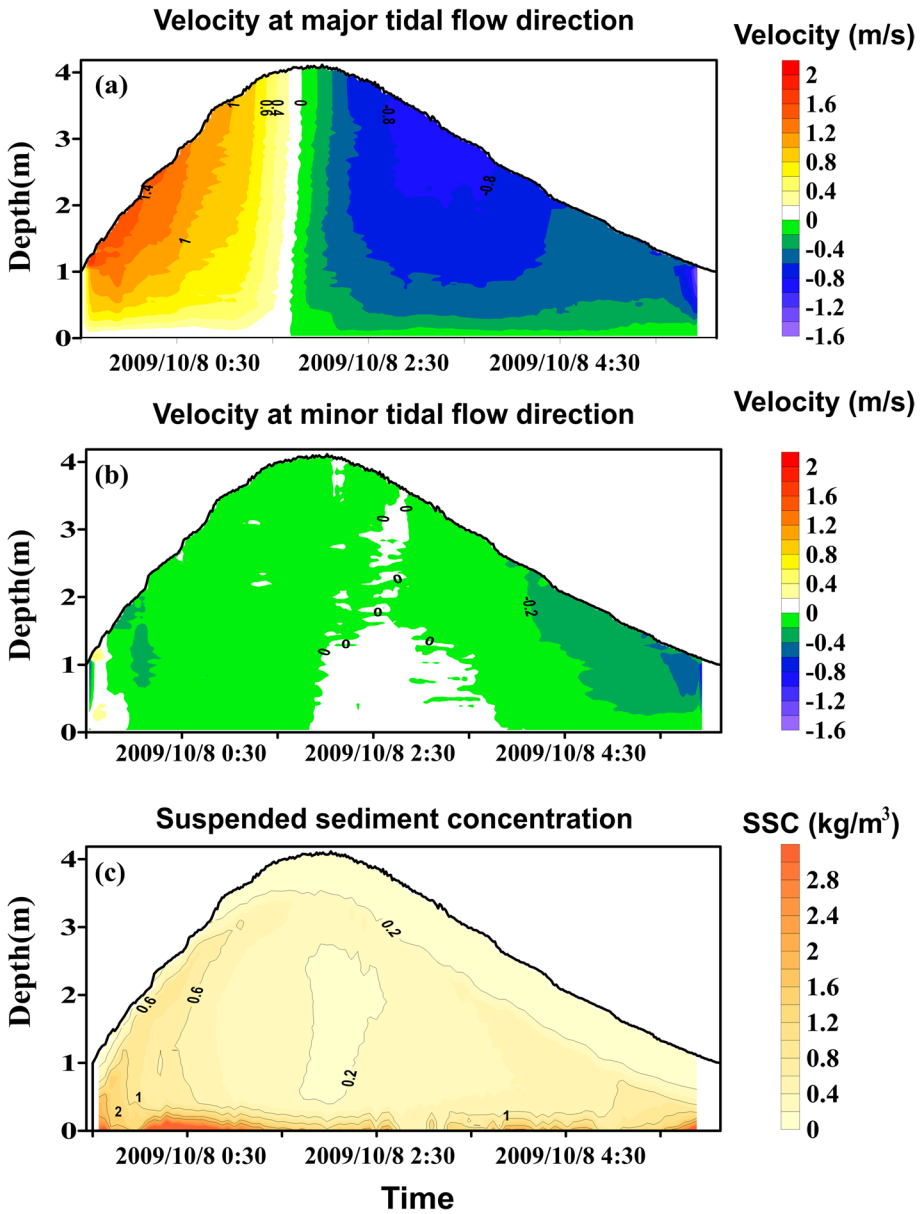

Fig. 6 Time series of velocity and SSC vertical profiles at station 4 over one tidal cycle from 23:26, Oct. 7th, 2009 to 5:40, Oct.8th, 2009. **a** major velocity (351° from north) **b** minor velocity (81° from north) **c** SSCs

distinct from former studies (Wu et al. 2008), which may be attribute to local topography. Consistent with tidal currents, residual currents had larger north-south components compared with west-east components. Residual currents on the upper flat (station 1 and 3) directed seaward east, while on the lower flat (station 2 and 4), residual currents directed landward west. This pattern of current indicated that ebb related residual current was dominant on the upper flat but flood related residual current was dominant on the lower flat. In addition, Stocks drift became more important in shallow water than deep water, responding to the magnified tidal deformation landward. Residual currents were much larger on tidal flat in Jianggang than that in Dafeng, which may be correlated to the stronger tidal currents and more complicated morphology on Jianggang tidal flat. Tidal deformation played a very important role on sediment dynamics on Jianggang tidal flat, showing as the large magnitude of Stocks drift. Despite the pattern of residual currents decreased landward (Xing et al. 2012), the complicated

Table 1 Calculated residual currents (m/s) and their north and east components over 1 tidal cycle at the four stations

Station	Direction	Eulerian	Lagrangian	Stocks drift
1	North	0.08133	0.08913	0.00780
	East	0.04959	0.05518	0.00559
2	North	0.10399	0.10939	0.00540
	East	−0.04724	−0.04862	−0.00137
3	North	0.21214	0.34610	0.13396
	East	0.08204	0.12202	0.03997
4	North	0.18024	0.19136	0.01112
	East	−0.10307	−0.09139	0.01167

morphology in Jianggang led to a larger residual current observed on the upper flat station 3 comparing to lower flat station 4.

4.3 Suspended sediment mean and instantaneous flux

4.3.1 Mean suspended sediment flux (SSF) over one tidal cycle

Sediment flux was decomposed and all terms were calculated at station 2, 3 and 4 (SSCs at station 1 was not recorded, Table 2), which helps us to understand the importance of different processes on suspended sediment transport at different stations. There are some common characteristics among all stations:

(1) *T1* was the largest of all components, demonstrating Eulerian current was the dominant force in determining net suspended sediment transport.
(2) SSF was transported to north at all stations and the magnitude was larger than that in the east, consistent with major current direction.
(3) *T6* and *T7* were very small compared to *T1*, so the vertical variations of current and suspended sediment did not cause a large sediment flux on lower tidal flats although SSCs were much larger in bottom water layer than overlying water layers. No correlated data was recorded on the higher tidal flat.

Some distinctive characteristics were observed among the three stations in Dafeng and Jianggang tidal flats:

(1) The values of total SSF on the tidal flat in Jianggang were much larger than those in Dafeng, probably because of the stronger current and higher SSCs observed at Jianggang than Dafeng.
(2) The values of SSF at station 3 was extremely larger than those at station 2 and 4, indicating that the strong dynamics and shallow water depth were in favor to initiate and move sediment, and upper flats played an important role in redistributing sediment on intertidal flats.
(3) Suspended sediment transported landward at lower flat stations 2 and 4 (with positive eastern component), which changed to become landward at station 3 (with negative western component). The changes of sediment transport direction were in favor to accumulate sediment in the middle of tidal flats.
(4) *T2* at station 3 was one or two magnitude larger than other stations, indicating that although Eulerian current had a predominant role in transporting sediment at the lower flat, in the shallow upper flat, Stocks drift and phrase lags played more important roles, probably owing to the non-line effects and the deformation of tides in shallow water area.
(5) *T6*, *T7* and *T4* were relatively larger than other terms at station 2, representing the importance of vertical variations and tidal phase lags, however, at station 3, *T2* was very large, showing that Stocks drift had a great influence on suspended sediment transport, the relatively large values of *T2*, *T3* and *T4* demonstrated that tidal phase lags were also important.

Table 2 Mean sediment flux of suspended sediment over 1 tidal cycle at station 2, 3, and 4

Station	Direction	*T1*	*T2*	*T3*	*T4*	*T5*	*T6*	*T7*	Total SSF
2	North	0.02096	0.00319	−0.00032	−0.00582	0.00101	0.00549	−0.00875	0.01576
	East	−0.01691	−0.00159	0.00026	0.00095	0.00016	0.00015	0.00864	−0.00834
3	North	1.16560	0.73601	0.15464	0.21928	0.23666			2.51218
	East	0.450784	0.21962	0.05980	−0.04321	0.22921			0.91621
4	North	0.28098	0.01734	−0.03848	−0.13490	−0.00562	−0.00069	0.00305	0.12168
	East	−0.16068	0.01820	0.02200	−0.00934	−0.00769	0.00034	−0.00030	−0.13747

T1 to *T7* and total SSF are in the unit of kg/m/s

4.3.2 Instantaneous flux of suspended sediment over one tidal cycle

Based on Eq. 5, instantaneous flux of suspended sediment were decomposed into five constituents over a tidal cycle (Fig. 7). Sediment flux were transported to south-east direction during the flood tide and north-west direction during the ebb tide, but the values of sediment flux during the ebb tide were much larger than that during the flood tide, resulting in the net sediment flux to northwest (Table 2). Although Eulerian residual current played a predominant role in determining total residual current, the instantaneous flux told a different story. *E1* represented the effect of water level changes determined by tidal mean velocity, and the value reached the maximum when water level was highest. *E2* described the effect of depth and SSCs, and the values changed very little except an extremely large value appeared near the end of the tidal cycle, which was due to an extreme values of velocity and SSC at that time. *E3* had a similar trend as *E* with a larger magnitude comparing to other terms, which was caused by variations of velocity within the tidal cycle. *E4* showed the joint effect of velocity and suspended sediment variations within the tidal cycle. Its values were relatively small except the large values near the end, showing that tidal variations played a great role on determining sediment transport in very shallow water, but became less important when water depth was large. *E5* demonstrated the effect of vertical shear stress and diffusion, which changed greatly within the tidal cycle in the north-south direction. *E5* was relatively steady and directed to north during the flood tide and turned to south with large temporal variations during the ebb tide, depicting the vertical profiles during the ebb tide was more complicated. The term *E5* did not highly influence sediment transport as its values were small. In all, although several instantaneous flux components changed significantly within the tidal cycle, most of them did not produce net sediment transport because of their small values or their counteract effects within the tidal cycle, tidal mean flux transport, on the other hand, played a predominant role in determining net sediment transport flux.

The instantaneous flux of suspended sediment at station 3 (Fig. 8a-e) and 4 (Fig. 8f-k) on the tidal flat in Jianggang was 1 magnitude larger than the flux measured on the tidal flat in Dafeng. The instantaneous flux of suspended sediment at station 3 was characterized by larger values in both east-west and north directions, and sediment was transported to south-west during the flood period but north-east during the ebb period, followed by a long-term small values at the end of the ebb tide. Sediment flux were mostly directed to north over the entire tidal cycle, which gradually changed from west to east, showing the characteristics of rotatory flow. Similar to Dafeng, *E3* had the maximum value among all components and determined the pattern of instantaneous sediment flux variations, showing that

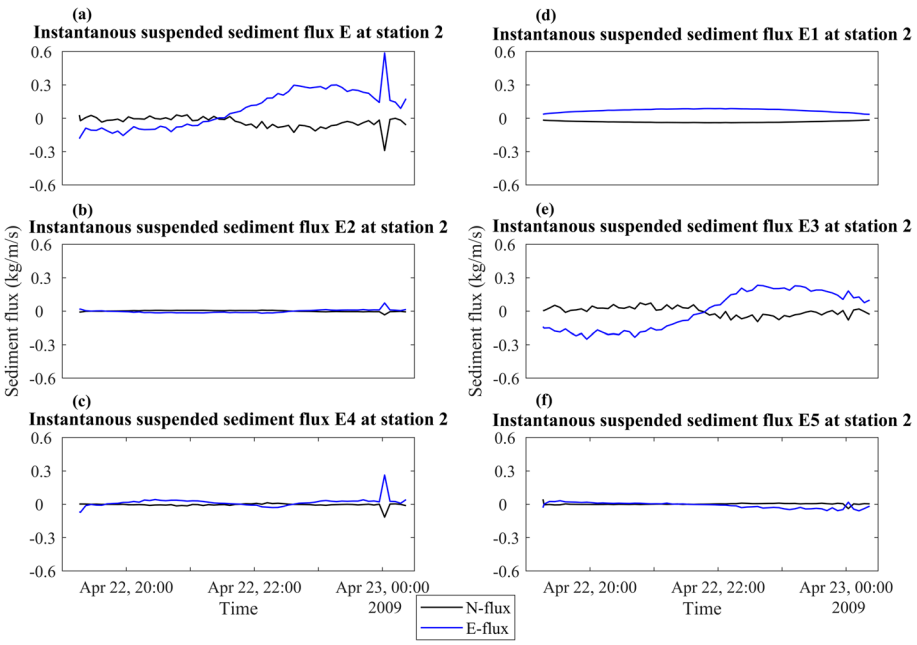

Fig. 7 Instantaneous suspended sediment flux at station 2 on tidal flat in Dafeng over 1 tidal cycle (showing in red dash rectangle in Fig. 3). **a**, **b**, **c**, **d**, **e**, **f** represents *E*, *E1*, *E2*, *E3*, *E4*, *E5* at station 2, and E shows the total instantaneous suspended sediment flux

variations of velocity within the tidal cycle played the predominate role in determining instantaneous sediment flux. Although *E3* and *E4* had larger values than other components, their counteracting effect led to the most important role of *E1* in determining net sediment transport flux over the tidal cycle.

At station 4 the instantaneous flux of suspended sediment was evidently smaller than that at station 3. The south-east component had smaller changes within the tidal cycle comparing to that at station 3, indicating that on the lower part of intertidal flat, lateral sediment transport cross the tidal flat was smaller than that on the upper flat. Distinct from other stations, *E4* at station 4 was much larger than *E3*, showing that variations of velocity and SSCs in the tidal cycle played a more important role in determining instantaneous sediment flux in the tidal cycle. In all, although instantaneous flux had large temporal variations, the tidal mean flux of suspended sediment at both Dafeng and Jianggang were mainly determined by *E1* over the entire tidal cycle (Figs. 7 and 8).

4.4 Vertical profiles of tidal flat and median grain size

The tidal flat in Dafeng is characterized with a convex-up profile, which is usually seen on accretion-dominated environment, while the tidal flat in Jianggang had a concave-up shape, which is usually seen on erosion-dominated tidal flat (Postma 1954; Strasten and Kuenen 1958) (Fig. 9). The median grain size of sediment coarsened seawards on both tidal flats, but was more uniformly distributed along Jianggang tidal flat profile, while more spatial variations were observed along Dafeng tidal flat profile. For instance, grain size along Dafeng profile coarsened between 400 m to 1500 m from seawall, in corresponding to the most convex-up shape of the elevation profile. In Jianggang tidal flat, the radical tidal current field leads to complicated patterns in bed slope and grain size

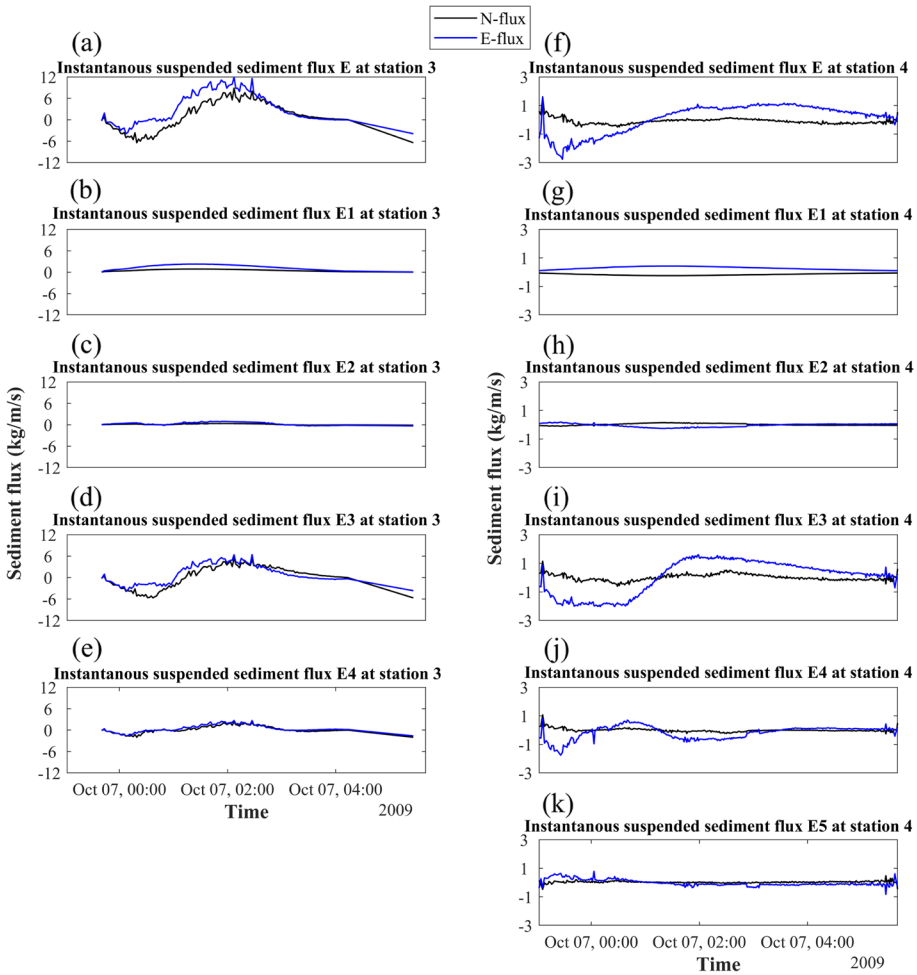

Fig. 8 Instantaneous flux of suspended sediment at station 3 and 4 in Jianggang over 1 tidal cycle. **a**, **b**, **c**, **d**, **e** represent *E*, *E1*, *E2*, *E3*, *E4* at station 3, respectively; **f**, **g**, **h**, **i**, **j**, **k** represents *E*, *E1*, *E2*, *E3*, *E4*, *E5* at station 4, respectively

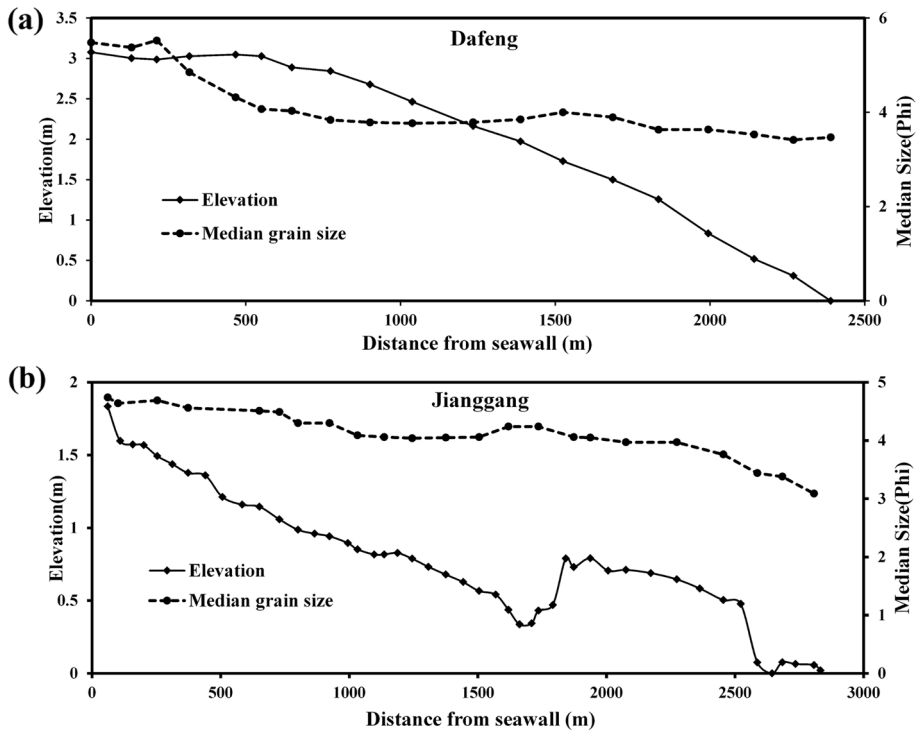

Fig. 9 Bed elevation and median grain size distribution along the tidal flat profiles in **a** Dafeng (P1); **b** Jianggang (P2)

distribution along tidal flats. More discussions on tidal flat profile and grain size are shown in Section 5.1.

5 Discussions

5.1 Offshore hydrodynamics and tidal flat profiles

In order to analyze the mechanisms for the significant differences in morphodynamics between Dafeng and Jianggang tidal flats, we acquired water depth and velocity time series over 1 month from a validated Delft3D model (Ni 2014) offshore of Dafeng and Jianggang tidal flats within deep water channels. Station s5 was located offshore of Dafeng tidal flat within Xiyang channel, where mean water depth was around 13 m (Fig. 1b). Station s6 and s7 were derived offshore of Jianggang tidal flat at the south end of Xiyang channel (s6, mean water depth of 3 m, Fig. 1c) and the west end of Huangshayang channel (s7, mean water depth of 8 m, Fig. 1c), respectively. In general, tidal currents were stronger and more symmetric at offshore stations. Velocities were highly controlled by water depth where the deepest station had the largest velocities (Fig. 10b). s5 and s6 were located at the end of deep channels where flow started to be highly impacted by channel directions while station 4 was less influenced by channel directions as it was located in the middle of the deep Xiyang channel. Although s5 had the largest velocities than other two stations, tidal currents at Dafeng tidal flat were much smaller than that at Jianggang. One reason was that Dafeng tidal flat had a convex-up shape, which favored to tidal current energy dissipation on the lower tidal flat, therefore, velocities were usually highest in the middle tidal flat (Hanssen et al. 2022). Jianggang profile was concave-up, and the comparatively large water depth along tidal flat profile favored energy transferring to the upper flat. Another reason, which was probably the most important reason was that Dafeng station was protected by two seawalls in both north and south (Fig. 1b) perpendicular to major tidal current direction, which effectively blocked tidal energy from transferring onto the tidal flat. Tidal currents on the lower tidal flat at Dafeng (station 2) followed the same pattern as offshore deep water station (Figs. 3d and 10b) with a smaller magnitude, showing that offshore currents largely control the current patterns on lower tidal flats. At Jianggang, tidal currents at the lower flat (station 4) was similar to the flow pattern at s6 in Xiyang Channel, but largely different from station s7 in Huangshayang channel. However, the rotatory pattern on the tidal flat may be impacted by tidal currents from Huangshayang channel and other big channels. The converging effects of tidal currents caused complicated

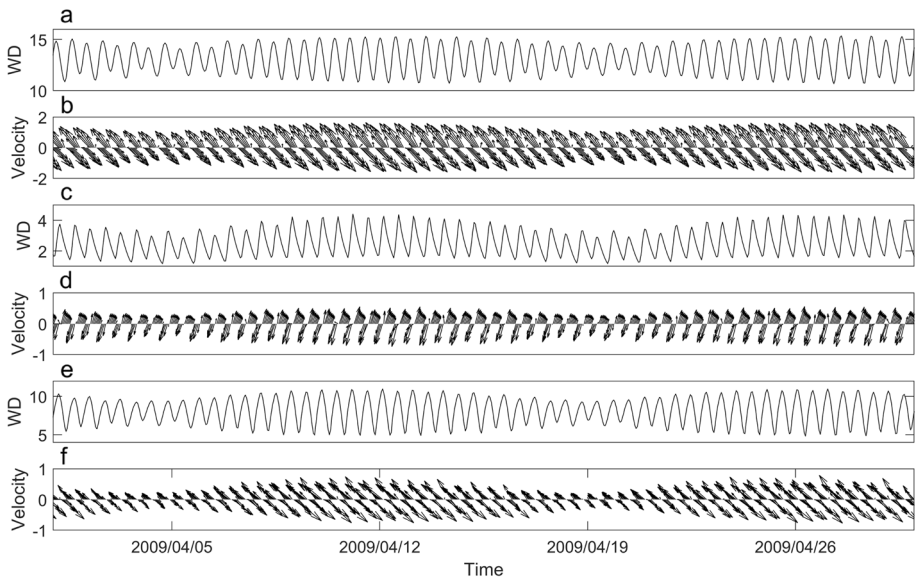

Fig. 10 Hydrodynamics offshore of Dafeng and Jianggang tidal flats derived from a validated Delft3D model (Ni 2014). **a** water depth at station 5 in Xiyang channel offshore of Dafeng tidal flat; **b** velocity at station s5 in Xiyang channel offshore of Dafeng tidal flat; **c** water depth at station 6 in Xiyang channel offshore of Jianggang tidal flat; **d** velocity at station 6 in Xiyang channel offshore of Jianggang tidal flat; **e** water depth at station s7 in Huangshayang channel offshore of Jianggang tidal flat in the south; **f** velocity at station s7 in Huangshayang channel offshore of Jianggang tidal flat in the south. The locations of station s5, s6, s7 are shown in Fig. 1b, c

hydrodynamics on Jianggang tidal flat, which significantly influenced morphology of the tidal flat.

In response to hydrodynamics, sediment grain size and bed elevation profiles adjust accordingly. The phenomenon of sediment coarsen seaward was first observed by Hantzechel in 1939, and has been attributed to delay effect (Postma 1954, 1961, 1967; Strasten and Kuenen 1958). According to Postma (1954), delay effect works when grain size is between 8 to 100 μm, and the asymmetry of current over time enhances this effect. They also suggested that, other factors, such as current direction that is parallel to the shoreline, and current speed which increases fast during flood tides, but decreases slowly during ebb tides, would lead to reinforcement of delay effect. All of these mentioned aspects fit tidal flats in Jiangsu. Figures 3 and 5 showed that the time period that the current speed was smaller than 0.05 m/s, considered as slack time, lasted much longer in the upper flat than the lower flat, resulting in deposition of fine sediment on the upper flat. Meanwhile, the spring and neap tidal cycles cause periodic submergence and deposition of sediment in the upper flat during spring tides, while dehydration and compaction happen during neap tides, resulting in high bed resistance to erosion on high tidal flats when it will be re-submerged in the next spring cycle. The combination of the two aspects are the reason for the specific grain size distribution on the tidal flat in Jiangsu. Dafeng tidal flat does not have as strong tidal asymmetry as Jianggang between flood and ebb tides (Fig. 6a), and the tidal currents and tidal creeks are distributed vertically to shoreline (Fig. 1c), which are unfavorable for the formation of sediment sorting from upper to lower tidal flat. Therefore, the coarsen trend of sediment at Dafeng tidal flat was not as obvious as that at Jianggang (Fig. 9).

The bed profiles at the two tidal flats have very distinctive features. W. Roberts and R. Kirby suggested that accretion-dominated profile tends to be high and convex, while erosion-dominated profile tends to be low and concave (Roberts et al. 2000; Kirby 2000; Liu et al. 2011), demonstrating that the tidal flat in Dafeng was a typical accretion-dominated profile, but that in Jianggang was erosion-dominated. The differences can be attributed to their different residual currents and sediment transport patterns. As shown in Fig. 1b, coastal line at Dafeng is directed NW ~ SE (about 156 ~ 336°). At station 1, the Lagrangian residual current was about 32°, which can be decomposed to the paralleling coastal current of 0.059 m/s, and the perpendicular seaward current of 0.087 m/s. At station 2, the direction of net SSF was about 332°, and the Lagrangian residual current was about 336°, showing a small net sediment transport landward. The much larger residual current at station 2 than station 1, and the total SSF directed to shore, resulting in the accretion–dominated profile. Comparatively, the Jianggang tidal flat coastline was in

the north-south direction, and the sediment transport directions at station 3 and 4 was 20° and 312°, respectively. The seaward residual current at station 3 with the scale of 0.122 m/s and landward current at station 4 with the scale of 0.0914 m/s, results in the net sediment flux from land to sea. This may explain the different vertical profiles on tidal flats in Dafeng and Jianggang. Furthermore, the slope of profiles are related to tidal range, SSCs at the boundary layer, and the wave height (Roberts et al. 2000). The larger tidal range at Jianggang favors to form steepe slope profiles, while the larger SSCs were favorable to form flatter profiles.

Another feature on the tidal flat profile in Jianggang was the sudden increased elevation at the lower flat (Fig. 9b), located between two tidal creeks. There has very little studies to explain the formation mechanism of the high-elevated land surrounding tidal creeks. We infer there are several reasons. One mechanism is sediment deposition alike river floodplain. The flooding tides flow from tidal creeks to surrounding flat at the beginning of flood tides, and the abrupt reduction of depth causes sudden decrease in velocity from channels to flat and causing deposition on surrounding flat. Another reason may be correlated to the tidal creeks parallel to shoreline. During ebb tides, most of water flows from upper land to the tidal channel close to land, and only very little water goes through the area between two channels, so this area is protected from the strong flow caused high bottom shear stress observed at the end of ebb tides (Figs. 3 and 5). The radical current field and sand ridge systems must also have influenced the morphology on Jianggang tidal flat, causing the formation of this high elevated land at the lower tidal flat profile. These sudden increase in elevation at lower tidal flats is very harmful and have caused severe deaths in the local county. Beachcomber who search for seafood when tides are low may be trapped on these high land far from shore at the beginning of flooding tides as they assume that elevation on tidal flat decrease seawards. As a result, no enough time for them to walk back to safe zone when flooding tides start to flood these high lands in the lower flat.

5.2 Human's impact on tidal flat morphology

Land reclamation is the most predominant factor that influences tidal flat morphology along China coast in the recent years (Xu et al. 2022). Tidal flats in both Dafeng and Jianggang have experienced significant changes due to seawall constructions. Seawall projects have underwent 3 cycles on Dafeng tidal flat, in 1978, 2000, and 2008, respectively. Accordingly, the tidal flat profile have been shortened significantly (Wang et al. 2012), forcing tidal energy to diminish within a shorter distance. The result is accumulation on upper flat and erosion on lower flat, which have been observed widely along China coast (Wang et al. 2020). Wang et al. (2012) showed a clear trend of the tidal flat profile steepen over time with the construction of seawall at Dafeng. Two seawalls were built in the north and south sides of our observation stations at Dafeng tidal flat, protecting the flat from offshore oceanic forces, which was in favor to sediment deposition on tidal flat. Jianggang tidal flat is characterized with complicated hydrodynamics and morphology and unsteady tidal creeks. A new seawall has been built between 2011 and 2012 (Fig. 1c), and the upper flat on profile P3 has been reclaimed. The shortened profile made the tidal flat more influenced by the strong offshore radical flow field, and big channel switches have been observed within the recent years (Wang et al. 2020).

In order to explore the mechanisms how seawall influences tidal flat morphology, an idealistic rectangular model was set up with 11,430 grid. Grid resolution decreased from coast to offshore and from center to north and south boundary, with the highest resolution of 120 m at coast. Model bathymetry was set up with uniform slope of 0.0017 from 3.5 m above mean sea level to water depth of 14 m, then slowly increased to 17 m. To better represent the hydrodynamic conditions of Jiangsu tidal flat, the tidal boundary was set up using the TPXO global tidal model (Egbert and Svetlana 2002) which provided tidal condition offshore of Dafeng tidal flat. One non-cohesive sediment class and one cohesive sediment class were included in the model, and correlated important parameters, such as the median grain size of non-cohesive sediment, critical shear stress for erosion, were derived from the former validated model (Ni 2014). The model was first run for 75 years with morphological acceleration factor of 100 to get a comparatively equilibrium condition. And then four idealistic cases were set up and run for another 75 years to explore the importance of seawalls on tidal flat morphology (Table 3).

The idealistic model showed that tidal flat prograded fast to offshore from initial bathymetry under the influence of tidal currents parallel to coast (Fig. 11). A big channel was formed in the south of the domain parallel to tidal current direction. The major sediment source was offshore erosion as depth in the offshore area decreased significantly with time (Fig. 11a, b). The tidal flat kept prograding in the next 75 years, but the pattern varied for different cases. No obvious changes occurred when the seawall was located very close to the shore (bed elevation of 1.7 m above mean sea level), as this area was mostly unsubmerged (Fig. 11c, d). When sea wall was built further offshore (bed elevation of 0.8 m blow mean sea level), more deposition was observed on tidal flat, although the pattern was similar

Table 3 Idealistic model set up to study the impact of sea walls on tidal flat morphology

Cases	Sea wall set up
Base	no sea wall
Seawall_v1	Sea wall parallel to coast, located close to shore (see location in Fig. 11)
Seawall_v2	Sea wall parallel to coast, located farther to shore (see location in Fig. 11)
Seawall_v3	Two sea walls, one parallel to coast, and one vertical to coast (see location in Fig. 11)

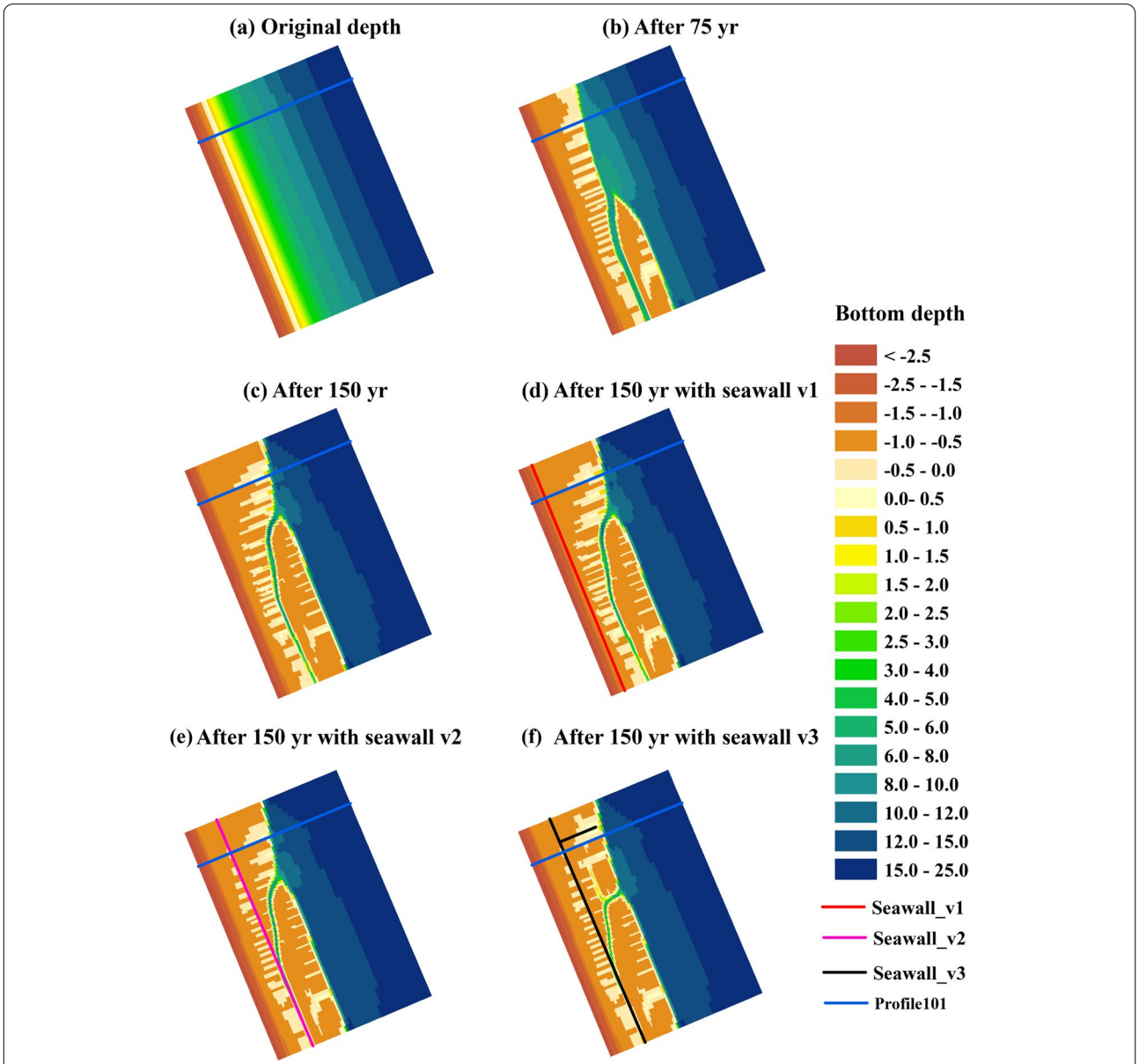

Fig. 11 Idealistic model bed elevation showing morphological evolution of tidal flats: **a** model initial bed elevation; **b** model bed elevation after 75 years, used as the starting condition for cases shown in Table 3; **c** model bed elevation after 150 years without seawall; **d** model bed elevation after 150 years with seawall, and seawall was shown as the red line; **e** model bed elevation after 150 years with seawall located farther offshore, shown as the magenta line; **f** model bed elevation after 50 years with two seawalls, one is parallel to coast, and the other one is perpendicular to coast, shown as the black lines. The blue line shows the profile P101 along which vertical elevation profile and velocity at flood maxima was extracted for further analysis

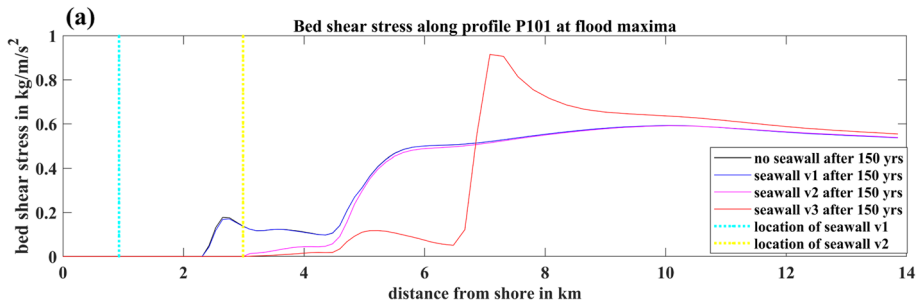

Fig. 12 Bed shear stress along profile P101 at flood maxima 75 years since model setup (location in Fig. 11)

to case seawall_v1. The sea wall located perpendicular to shore had a more significant influence on morphology, shown as more deposition and new land formation in the south of the seawall, demonstrating that the seawall perpendicular to tidal current direction had significantly reduced the strength of local hydrodynamics by blocking major tidal current from approaching the tidal flat, in favor to sediment deposition and tidal flat progradation, which was similar to the case of Dafeng tidal flat. Bed shear stress along profile P101 (location in Fig. 11) clear showed the reduction in bed shear stress due to seawall construction on the tidal flat (Fig. 12). The bed shear stress increased at offshore area (6-8 km from shore) in the case seawall_v2, demonstrating more sediment would be eroded from offshore, which provided sediment source to tidal flat to support its progradation. In Jianggang, on the other hand, the influence of seawall is less significant compared to Dafeng, shown as similar hydrodynamics observed on the lower tidal flat and offshore station, the reason is that only one seawall parallel to shore has been built, which did not block the way for radial tidal current to approach the tidal flat. Besides, the radical distributed offshore tidal current field made it harder to block the tidal current from approaching surrounding tidal flats.

The difference between the idealistic model and tidal flat along Jiangsu coast is that the morphological changes have not reached an equilibrium in the idealistic model, therefore, tidal flat kept prograding over time by eroding offshore sediment, showing as significantly morphological changes over time. Comparatively, the influence of seawall became less important. But the idealistic model did show that the construction of seawalls significantly change local tidal flat morphology (Fig. 11e, f). Jiangsu tidal flat systems, for which tidal flats has reached in an equilibrium before seawall projects, the widely distributed and frequently constructed seawalls is the major environmental factor that changes significantly with time. Therefore, human intervene became the most important factor controlling tidal flat morphological evolution. Since 2020, a new policy has been placed to stop land reclamation along China coast, this policy will significantly influence coastal morphology, and tidal flat evolution along China coast. Sea level rise, which accelerated over time, would be another important factor influencing tidal flat morphodyanmics in the future.

6 Conclusions

Hydrodynamics and sediment transport patterns along two tidal flats located in different area with distinct human interferences have been observed to study the spatial variations in tidal flat features along Jiangsu coast, China. The hydrodynamics on tidal flat was determined by offshore tidal force, and then largely modified by local morphology, especially the construction of seawalls. The two tidal flats share some common features, such as the tidal current asymmetry and rotatory current pattern which magnified landwards, and high SSCs observed close to bottom and at the beginning and ending periods of a tidal cycle, due to tidal intrusion front. Eulerian residual current was the major contributor of Lagrangian residual current over a tidal cycle. Residual sediment flux directed landwards on the lower flat and seaward on the upper flat, in favor to sediment deposition in the middle flat. Sediment transport was much active on the upper flat than the lower flat, and Stocks drift played a more vital role in shallow water. Instantaneous flux have much larger variations over a tidal cycle than mean flux, and variations of velocity and SSCs in the tidal cycle played the most vital role, however, its counteract effects leading to the result that Eulerian flux became the most important component to determine the net sediment flux.

The distinctive features between the two tidal flats include the much stronger currents in Jianggang than Dafeng, although Dafeng offshore current was stronger than Jianggang. The reason for the small tidal current at Dafeng tidal flat was the construction of seawalls in the north and south of the tidal flat, which significantly reduced hydrodynamics on the tidal flat area. This has

been validated by an idealistic model which showed that seawall built perpendicular to shoreline and tidal currents had a larger impact on tidal flat morphology evolution, which caused deposition and tidal flat progradation in the hidden area. Tidal asymmetry and SSCs vertical variations were more obvious in Jianggang than in Dafeng, attribute to its stronger tidal currents and complicated offshore radical current field. Dafeng tidal flat is in the process of accretion with convex-up shape and landward net sediment flux, while Jianggang tidal flat is in the process of erosion with concave-up shape and net offshore sediment flux. The high elevated land located between two tidal creeks at the lower flat of Jianggang may be formed due to the creek directions parallel to the shore, and sediment deposition at the beginning of flood tides, which have caused severe accidents on benchcombers' lives. More studies are needed to understand the mechanisms for the formation of these high elevated lands at the lower tidal flat.

Acknowledgements
We thank Jiasheng Li, Xiao Wei, Zhishuai Liu, Longjiang Ran, Jiabi Du, Dandan Wang, Jun Chen for their assistances in collecting field data and doing laboratory analysis.

Authors' contributions
FX: research design, data collection, data analyses, data interpretation, manuscript writing. JJ: data interpretation, manuscript writing. YPW: research design, data interpretation, manuscript writing, funding. The author(s) read and approved the final manuscript.

Funding
This study is supported by This study was financially supported by the National Natural Science Foundation of China (41625021, 42006149), Jiangsu Special Program for Science and Technology Innovation (JSZRHYKJ202106), and Jiangsu coastal geological resources and environmental multi-factor monitoring network optimization and dynamic controlling (202146).

Availability of data and materials
The datasets used and/or analyzed during the current study are available from the corresponding author on reasonable request.

Declarations

Competing interests
Author Ya Ping Wang is a member of the Editorial Board for Anthropocene Coasts. He was not involved in the journal's review of, or decisions related to, this manuscript. The authors have no other competing interests to disclose.

Author details
[1]State Key Laboratory of Estuarine and Coastal Research, School of Marine Sciences, East China Normal University, Shanghai 200062, China. [2]Ministry of Education Key Laboratory for Coast and Island Development, School of Geographic and Oceanographic Sciences, Nanjing University, Nanjing 210093, China.

Received: 2 August 2022 Revised: 10 October 2022 Accepted: 20 October 2022
Published online: 30 November 2022

References

Barbier EB, Koch EW, Silliman BR, Hacker SD, Wolanski E, Primavera J, Granek EF, Polasky S, Aswani S, Cramer LA (2008) Coastal ecosystem-base management with nonlinear ecological functions and values. Science 319:321–323
Bartholdy J, Aagaard T (2001) Storm surge effects on a back-barrier tidal flat of the Danish Wadden Sea. Geo-Mar Lett 20(3):133–141
Dionne JC (1988) Characteristic features of modern tidal flats in cold regions. In: de Boer PL (ed) Tide-influenced sedimentary environments and facies. D. Reidel Pub. Co, Dordrecht, pp 301–332
Dyer KR (1997) Estuaries — a physical introduction (2nd edition). Wiley, Singapore, p 195
Egbert GD, Svetlana YE (2002) Efficient inverse modeling of barotropic ocean tides. J Atmos Ocean Technol 19(2):183–204
Eisma D (1997) Intertidal deposits: river mouths, tidal flats and coastal lagoons, Marine science series. CRC Press, Boca Raton, pp 507
Friedrichs CT (2011) 3.06 tidal flat morphodynamics: a synthesis. In: Wolanski EE, McLusky D (eds) Treatise on estuarine and coastal science. Academic, Pittsburgh, pp 137–170
Friedrichs CT, Aubrey DG (1996) Uniform bottom shear stress and equilibrium hypsometry of intertidalflats. In: Pattiaratchi C (ed) Mixing in estuaries and coastal seas, coastal and estuarine studies, vol 50. American Geophysical Union, Washington DC, pp 405–429
Gao S (2009) Modeling the preservation potential of tidal flat sedimentary records, Jiangsu coast, eastern China. Cont Shelf Res 29(16):1927–1936
Ghosh S, Mishra DR, Gitelson AA (2016) Long-term monitoring of biophysical characteristics of tidal wetlands in the northern Gulf of Mexico-a methodological approach using MODIS. Remote Sens Environ 173:39–58
Hanssen JLR, van Prooijen BC, Volp ND, de Vet PLM, Herman PMJ (2022) Where and why do creeks evolve on fringing and bare tidal flats? Geomorphology 403:108182. ISSN 0169-555X
Jin HR, Huang CQ, Lang MW, Yeo I-Y, Stehman SV (2017) Monitoring of wetland inundation dynamics in the Delmarva Peninsula using Landsat time-series imagery from 1985 to 2011. Remote Sens Environ 190:26–41 ISSN 0034-4257
Ke X, Li SE, Xu L (1990) Ecosystem features and exploitation model of the tidal flats of Dafeng, Jiangsu, China, Final report of the research programme supported by the Young Scientist Award of MAB, UNESCO, pp 45
Ke X, Yu G (1990) Impacts of large rivers and human beings' activities on Jiangsu tidal fiats. In: Proceedings of the 5th MICE Symposium for Asia and the Pacific. University Press, Nanjing, pp 36–49
Kirby R (2000) Practical implications of tidal flat shape. Cont Shelf Res 20:1061–1077
Koch EW, Barbier EB, Silliman BR, Reed DJ, Perillo GME, Hacker SD, Granek EF, Primavera JH, Muthiga N, Polasky S, Halpern BS, Kennedy CJ, Kappel CV, Wolanski E (2009) Non-linearity in ecosystem services: temporal and spatial variability in coastal protection. Front Ecol Environ 7:29–37
Le Hir P, Roberts W, Cazaillet O, Christie M, Bassoullet P, Bacher C (2000) Characterization of intertidal flat hydrodynamics. Cont Shelf Res 20(12-13):1433–1459
Li CX, Wang L, Li P (1979) Preliminary study of the facies distribution in the Changjiang delta. J Tongji Univ 3:1–14 (in Chinese with English abstract)
Li CX, Zhao J (1995) Study progress and dispute of Qianggang RSR in the northern Jiangsu. Mar Sci 4:57–60 (in Chinese with English abstract)
Liu XJ, Gao S, Wang YP (2011) Modeling profile shape evolution for accreting tidal flats composed of mud and sand: a case study of the central Jiangsu coast, China. Cont Shelf Res 31:1750–1760
Murray NJ, Phinn SR, Clemens RS, Roelfsema CM, Fuller RA (2012) Continental scale mapping of tidal flats across east Asia using the landsat archive. Remote Sens 4:3417–3426
Ni WF (2014) Numerical simulation on the geomorphodynamics of tidal channel-sand ridge-tidal flat system in the southern Yellow Sea. Master Thesis,. Nanjing University, Nanjing
Postma H (1954) Hydrograpy of the Dutch Wadden Sea. Arch Neerl Zool 10:405–511
Postma H (1961) Transport and accumulation of suspended matter in the Dutch Wadden Sea. Neth J Sea Res 1(1/2):148–190

Postma H (1967) Sediment transport and sedimentation in the Estuarine Environment. In: Estuaries, Lauff GH (ed). American Association for Advancement of Science, Washington, DC, pp 158–179
Ren ME (1986) Tidal mud flat. In: Ren ME (ed) Modern sedimentation in the coastal and nearshore zones of China. China Ocean Press, Beijing, pp 78–127
Ren ME, Yang RZ, Bao HS (1985) The outline of the physical geography of China. Shangwu Publication House, Beijing, pp 470 (in Chinese)
Ren SZ (1984) Land forming process of abandon Yellow River Delta and coastal plain. J Geol Sci 39(2):173–184 (In Chinese)
Roberts W, Le Hir P, Whitehouse RJS (2000) Investigation using simple mathematical models of the effect of tidal currents and waves on the profile shape of intertidal mudflats. Cont Shelf Res 20(10):1079–1097
Strasten LMJUV, Kuenen PLH (1958) Tidal action as a cause for clay accumulation. J Sediment Petrol 28:406–413
Wang AJ, Gao S, Jia JJ (2006a) Impact of the cordgrass Spartina alterniflora on sedimentary and morphological evolution of tidal saltmarshes on the Jiangsu coast, China. Acta Oceanol Sin 25(4):32–42
Wang XX, Xiao XM, Zou ZH, Chen BQ, Ma J, Dong JW, Doughty RB, Zhong QY, Qin YW, Dai SQ, Li XP, Zhao B, Li B (2020) Tracking annual changes of coastal tidal flats in China during 1986-2016 through analysis of Landsat images with Google Earth Engine. Remote Sens Environ 238:110987
Wang XY, Ke XK (1997) Grain-size characteristics of the extant tidal flat sediments along the Jiangsu coast, China. Sediment Geol 112:105–122
Wang Y (1983) The mudflat coast of China. Can J Fish Aquat Sci 40(1):160–171
Wang Y, Zhu DK (1990) Tidal flats of China. Quat Sci 4:291–300 (in Chinese with English abstract)
Wang YP, Gao S (2001) Modification to the Hardisty Equation regarding the relationship between sediment transport rate and particle size. J Sediment Res 71(1):118–121. https://doi.org/10.1306/032100710118
Wang YP, Gao S, Jia JJ (2006b) High-resolution data collection for analysis of sediment dynamic processes associated with combined current-wave action over intertidal flats. Chin Sci Bull 51:866–877
Wang YP, Gao S, Jia JJ, Thompson CEL, Gao JH, Yang Y (2012) Sediment transport over an accretional intertidal flat with influence of reclamation, Jiangsu coast, China. Mar Geol 291-294:147–161
Wang YP, Zhang RS, Gao S (1999) Velocity variations in salt marsh creeks, Jiangsu, China. J Coast Res 15(2):471–477
Wei W, Dai ZJ, Pang WH, Wang J, Gao S (2020) Sedimentary zonation shift of tidal flats in a meso-tidal estuary. Sediment Geol 407:105749
Wu XB, Wang YP, Pang SM (2008) Analysis of the transportation mechanism of suspended sediment and salt in the Changjiang River Estuary. Oceanogr Res 26(4):8–19 (In Chinese)
Xie W, He Q, Zhang K, Guo L, Wang X, Shen J, Cui Z (2017) Application of terrestrial laser scanner on tidal flat morphology at a typhoon event timescale. Geomorphology 292:47–58
Xing F, Wang YP, Wang HV (2012) Tidal hydrodynamics and fine-grained sediment transport on the radial sand ridge system in the southern Yellow Sea. Mar Geol 291-294:192–210
Xu N, Wang YQ, Huang CH, Jiang S, Jia MM, Ma Y (2022) Monitoring coastal reclamation changes across Jiangsu Province during 1984-2019 using landsat data. Mar Policy 136:104887
Zhang M, Dai ZJ, Bouma TJ, Bricker J, Townend I, Wen JH, Zhao TTG, Cai HY (2021) Tidal-flat reclamation aggravates potential risk from storm impacts. Coast Eng 166:103868
Zhang RS (1986) Characteristics of tidal current and sedimentation of suspended load on tidal mud flat in Jiangsu province. Oceanol Limnol Sin 17(3):234–245
Zhang RS (1992) Suspended sediment transport processes on tidal mud flat in Jiangsu Province, China. Estuar Coast Shelf Sci 35:225–233
Zhao BX, Liu YX, Wang L, Liu YC, Sun C, Fagherazzi S (2022) Stability evaluation of tidal flats based on time-series satellite images: a case study of the Jiangsu central coast, China. Estuar Coast Shelf Sci 264:107697
Zhou Z, Liang MJ, Chen L, Xu MP, Chen X, Geng L, Li H, Serrano D, Zhang HY, Gong Z, Zhang CK (2022) Proceses, feedbacks, and morphodynamic evolution of tidal flat-marsh systems: progress and challenges. Water Sci Eng 15(2):89–102

Publisher's Note